Occupied and unoccupied electronic band structure of WSe_2

Th. Finteis, M. Hengsberger,* Th. Straub, K. Fauth,† R. Claessen,‡ P. Auer, P. Steiner, and S. Hüfner
Fachrichtung Experimentalphysik, Universität des Saarlandes, D-66041 Saarbrücken, Germany

P. Blaha
Institut für Technische Elektrochemie, Technische Universität Wien, A-1060 Wien, Austria

M. Vögt, M. Lux-Steiner,§ and E. Bucher
Fakultät für Physik, Universität Konstanz, D-78434 Konstanz, Germany
(Received 14 November 1996)

An extensive investigation of the electronic band structure of the layered semiconductor 2H-WSe_2 is presented. Angular-resolved photoemission (ARPES) and angular-resolved inverse photoemission spectroscopy (ARIPES) data are compared to a full-potential fully relativistic density-functional calculation, yielding a very gratifying correspondence between the experimental and the theoretical data. The topmost valence band is found to behave differently than previous calculations have predicted, with the valence-band maximum (VBM) being situated at the sixfold degenerate K point of the Brillouin zone. Furthermore, the so-far-neglected spin-orbit interaction is shown to be essential for a correct description of the band structure in the vicinity of the VBM. The combination of ARPES and ARIPES spectra is used to determine the indirect and direct band gaps at various locations in the Brillouin zone and is compared to optical absorption data. We demonstrate that for a correct interpretation of the photoemission data it is crucial to account for band-bending effects, which are presumably caused by photon-induced surface defect states. Implications of our results for the optical and electrical transport properties will be discussed. [S0163-1829(97)02116-4]

I. INTRODUCTION

2H-WSe_2 belongs to the family of layered transition metal dichalcogenides (TMDC's) which display a wide variety of interesting physical properties[1] and have thus been of continuous interest for more than three decades. The pronounced anisotropy of these compounds results from the formation of MX_2 layers with strong covalent intralayer bonds, but only weak van der Waals coupling between adjacent layers. Like the other group VIb TMDC's, WSe_2 is a semiconductor.[1] It has been intensively studied as a potentially interesting material for photovoltaic applications because its optical absorption matches the solar spectrum quite well.[2,3] Furthermore, and in contrast to conventional semiconductors, the optical gap is determined by orbitals that contribute only weakly to the chemical bonding. As a consequence, the generation of electron-hole pairs by light absorption does not break any bonds, resulting in a remarkable stability against photocorrosion.[2]

Another puzzling property of WSe_2 has recently been discovered by scanning tunneling microscopy (STM).[4,5] Short voltage pulses applied to the tunneling tip are found to produce long-term stable and erasable surface modifications on a subnanometer scale, which can be probed again with the same tunneling microscope. This effect, which in principle allows the realization of a digital memory cell of atomic dimension, still lacks a detailed explanation.

Despite these interesting properties only relatively few investigations, both experimental and theoretical, have aimed at the determination of the underlying microscopic electronic structure. Most results were obtained from the related compound MoS_2, which was considered as a model compound for the semiconducting TMDC's with 2H structure, as early single-layer band calculations[6] demonstrated a strong similarity of their band structures. The first band-structure calculation based on density-functional theory (DFT) for these materials (MoS_2, $MoSe_2$, and WSe_2) was performed by Coehoorn *et al.*[7] A comparison to experimental results obtained from angle-resolved photoelectron spectroscopy (ARPES), however, was given only for $MoSe_2$.[7]

The compounds of the 2H-MoS_2 family are indirect-band-gap semiconductors and it has been generally believed that the valence-band maximum (VBM) lies at the center, i.e., at the Γ point of the Brillouin zone (BZ).[7] Very recently, we have presented experimental and theoretical evidence[8] that the VBM in WSe_2 is actually located at the sixfold degenerate K point of the BZ, in contrast to the predictions of the early band calculations. This is presently a controversial issue.[9]

This paper contains a comprehensive study of the occupied and unoccupied electronic band structure of 2H-WSe_2 by means of ARPES and angle-resolved *inverse* photoemission spectroscopy (ARIPES), respectively. We also present a DFT band-structure calculation, which, to our knowledge, is the first to use full potentials. It is demonstrated that, in contrast to what was reported earlier,[7,10] the inclusion of spin-orbit coupling is essential for a correct description of the band structure and can remove apparent discrepancies with experimentally observed behavior. We further show that for a correct interpretation of the ARPES data and, in particular, for the precise determination of the **k**-space location of the VBM it is crucial to account for time-dependent band-bending effects, which are caused by photon-induced defect states in the fundamental band gap. The combination

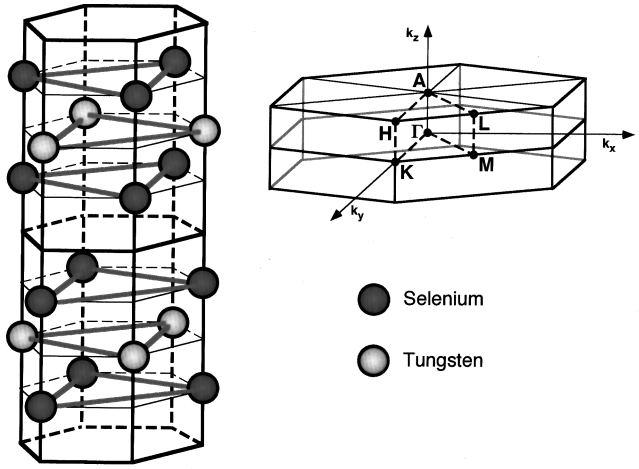

FIG. 1. Hexagonal unit cell and Brillouin zone of 2H-WSe_2.

of ARPES and ARIPES further allows the wave-vector-resolved determination of indirect and direct gaps in this semiconductor.

The remainder of this paper is organized as follows. In the next section we will review some of the physical properties of WSe_2 related to the electronic structure of this compound. We will particularly address its optical properties, since from our results we will be able to clarify some of the controversial issues discussed in the literature. After a brief outline of the experimental procedures in Sec. III we will describe our local-density approximation results in Sec. IV. Section V presents our spectroscopic results, which are to be discussed in Sec. VI. The conclusions will be given in Sec. VII.

II. STRUCTURAL AND ELECTRONIC PROPERTIES OF WSe_2

The crystal structure of 2H-WSe_2 belongs to the D_{6h}^4 space group. Figure 1 shows the symmetric unit cell, which contains two formula units located in two adjacent hexagonal Se-W-Se layers. Within each layer, the W atoms are coordinated in a trigonal prismatic arrangement. The lattice parameters are $a=3.282$ Å (in plane) and $c=12.960$ Å (perpendicular).[11] Two subsequent Se-W-Se sheets can be viewed as being displaced with respect to each other, forming an $ABABA\ldots$ hcp-type layer sequence. Alternatively, the crystal can be mapped onto itself by applying a nonprimitive translation by $c/2$ and subsequent rotation by $\pi/3$ (screw operation) with the screw axis located in the center of the unit cell and oriented along the c axis. This symmetry operation makes D_{6h}^4 a nonsymmorphic space group and implies selection rules for photoemission from the corresponding Bloch waves, which need to be taken into account for a correct interpretion of the ARPES data.[12] The (infinite) crystal thus is of sixfold symmetry, whereas each single WSe_2 sandwich layer as well as the surface is of threefold symmetry only.

The semiconducting nature of WSe_2 is most easily understood from a simple ionic picture,[1] in which the fully occupied Se $4p$ shell lies energetically below the W $5d$ states. The remaining electrons completely fill the W $5d_{z^2}$ orbital, which in the trigonal crystal field is split off from the rest of the d manifold, thus opening a gap between occupied and unoccupied states. While band-structure calculations[1,6,7,13] support the overall picture, they also find strong hybridization between Se $4p$ and W $5d$ states, resulting in a substantial covalent (i.e., nonionic) character of the chemical bonds.

In view of the layered crystal structure it seems, at first glance, not surprising to find a pronounced anisotropy in the electrical conductivity (e.g., $\sigma_\parallel/\sigma_\perp \approx 50-500$ at room temperature in p-type semiconducting crystals[14,15]). On the other hand, this observation seems not to be supported by the band-structure calculations so far available for WSe_2 and related materials,[1,6,7,13] which place the VBM at the center (i.e., Γ) of the Brillouin zone. Since at Γ the top of the valence band is mainly composed of W $5d_{z^2}$ and Se $4p_z$ states, considerable band dispersion is found not only along the layers but also perpendicular to them, resulting in a fairly *isotropic* band mass of the holes. In search of an alternative explanation for the observed two-dimensional transport properties early structural studies on WSe_2 (Refs. 16–18) claimed frequently observed stacking faults to be responsible for a strongly anisotropic carrier scattering. However, crystals of the type used in the present study have been subject to various investigations by STM,[4,5,19,20] and in no case have stacking faults been found,[21] indicating an improved crystal quality under state-of-the-art crystal-growth conditions. Therefore, the measured transport anisotropy still lacks a satisfactory explanation.

Already in 1977 WSe_2 was suggested to be a promising candidate for photovoltaic applications in electrochemical solar cells,[2] for which conversion efficiencies up to 17% have been reported.[22] For this reason the optical properties of WSe_2 have been intensively studied, mainly aiming at an understanding of photoexcitation and transport phenomena in an electrochemical environment. From the band calculations, WSe_2 is an indirect-band-gap semiconductor, in agreement with optical absorption experiments.[23] The size of the gap determined from experiment amounts to ≈ 1.2 eV at 300 K,[23] involving a transition from the VBM, formerly believed to be located at Γ, to the conduction-band minimum (CBM) about halfway between Γ and K (see Fig. 1 for a picture of the BZ).

The optical absorption across the *direct* band gaps is preceded by a series of excitonic peaks, the two most prominent ones being referred to as A and B excitons and observed at photon energies of 1.71 eV and 2.30 eV, respectively.[24] While there is some controversy about the assignment of the smaller exciton features to $n>1$ exciton states, it is generally agreed upon that the A exciton exhibits a binding energy of ≈ 0.1 eV or even less,[24,25] from which the (smallest) direct band gap can be inferred to amount to roughly 1.8 eV. From detailed studies of the exciton absorption[24–28] it was suggested to be related to direct transitions at the Γ point. From the measurement of the respective g factors it was concluded that the A and B excitons should have their origin in transitions out of spin-orbit split bands. Based on their band calculation, Coehoorn *et al.*[10] argued that for energetic reasons the direct band gap has to be situated at the K point (zone edge) of the BZ rather than at Γ. In line with the optical work, they suggested that spin-orbit splitting contributes to the energetic difference between the A and B excitons. However, they could not obtain convincing agreement of their

photoemission results on $MoSe_2$ with the corresponding optical exciton energies.

III. EXPERIMENTAL DETAILS

The photoemission spectra have been obtained using different angle-resolved electron spectrometers. Photon energy-dependent normal emission spectra were recorded using a Vacuum Generators (VG) Escalab spectrometer attached to the SX700-II monochromator at the BESSY synchrotron light source in Berlin. Angle and energy resolution were set to $\pm 1°$ and 100 meV, respectively. Off-normal ARPES data were obtained in our home laboratory on both a VG ADES 400 ($\pm 1.5°$/100 meV) and a VG Escalab Mk-II ($\pm 1.75°$/60 meV) spectrometer using the 21.22-eV radiation emitted from a conventional He discharge lamp. The latter system is equipped with a fully automated manipulator, allowing an independent variation of the azimuthal and polar angles of photoelectron detection and thus a large fraction of the 2π half space above the sample to be scanned.

The inverse photoemission experiment is a home-built apparatus consisting of a Stoffel-Johnson-type electron source[29] and a photon bandpass detector for 9.5-eV photons after Dose *et al.*[30] The design of the electron source was optimized by taking space-charge effects into account.[31] The resulting angle and energy resolution of the ARIPES spectrometer are $\pm 2°$ and 460 meV, respectively.

Establishing a common energy scale for photoemission and inverse photoemission spectra from a semiconductor is a nontrivial problem. This results from the fact that due to surface effects the position of the experimental Fermi energy in the band gap may vary from sample to sample, even when grown under similar conditions. Therefore, the ARIPES setup was additionally equipped with an angle-integrating photoemission unit, whose spectra were then compared to numerically momentum-integrated ARPES data. This allowed an energy alignment of ARPES and ARIPES data to within ± 0.1 eV.

The crystals were grown by the vapor transport method and typically several millimeters in diameter and a few hundred micrometers thick. They were glued onto Al sample holders, with electrical contact to the spectrometer achieved by applying graphite to the edges of the sample. In contrast to the use of conductive glue containing silver particles, which is known to cause Schottky barrier formation[32] on WSe_2, graphite contacts lead to an Ohmic behavior. Clean surfaces were prepared by *in situ* cleavage at a base pressure of typically better than 1×10^{-10} mbar. The azimuthal orientation of the crystals was determined either by x-ray diffraction using the Laue method or from photoelectron diffraction patterns obtained from excitations of core electrons. A few samples were oriented by low-energy electron diffraction (LEED).

The data presented here were obtained mostly on *p*-doped crystals. We also performed a few measurements on *n*-type material, which, however, showed no difference relative to those on *p*-type samples except for an energy shift related to the different Fermi level position in the band gap.

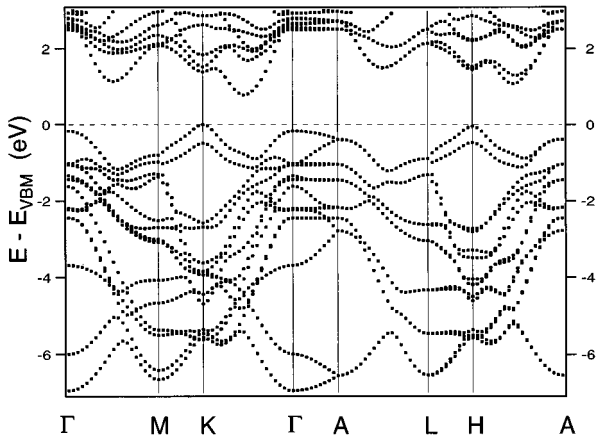

FIG. 2. Theoretical (LDA) band structure for WSe_2. Energies are given relative to the valence-band maximum at the *K* point.

IV. BAND-STRUCTURE CALCULATION

Despite the large number of TMDC band-structure calculations in the literature, only few theoretical studies address the properties of WSe_2 in concrete manner.[6,7,9] Until quite recently the calculation by Coehoorn *et al.*[7] was the only one of DFT type, using the local-density approximation (LDA) and the augmented spherical wave (ASW) method. According to these authors, the use of spherical potentials and only a restricted basis set may cause uncertainties in the band energies of up to 1 eV. Furthermore, this calculation fails to give a correct description of important aspects of the experimentally observed band structure. For this reason we have carried out a new state-of-the-art LDA calculation, which yields a much improved and in part remarkable agreement with the experimental results. Three major ingredients proved crucial for this success: the use of full potentials, restriction to the experimental structure parameters, and incorporation of spin-orbit coupling into the band structure.

Our band calculation has been performed using the linear augmented plane wave method, implemented in the WIEN-95 code,[33] including local orbitals for the high-lying ''semicore states.'' Exchange and correlation are treated within the LDA and the scalar relativistic equations were used to obtain self-consistency. In the final iteration spin-orbit coupling was included as a perturbation. In contrast to the previous LDA calculations,[7,9] no shape approximation to the potential or the charge density was made, and this is at the origin of the small but important differences between them and the present work. The resulting band structure is shown in Fig. 2.

The calculation was based on the experimentally determined structure parameters,[11] i.e., on the lattice constants given in Sec. II and a measured W-to-Se-layer distance of $z=0.129$ (in units of c), even though a total-energy minimalization (the other parameters held constant at their experimental values) yielded a slightly lower z of 0.126. We should note here that particularly the **k**-space location of the VBM depends critically on the actual z parameter used. For example, for the z value obtained from the energy optimization the highest occupied state is found at the Γ point, with the topmost eigenvalue at K being situated ≈ 80 meV below this value. Coehoorn *et al.*[7] used $z=0.121$ in order to ac-

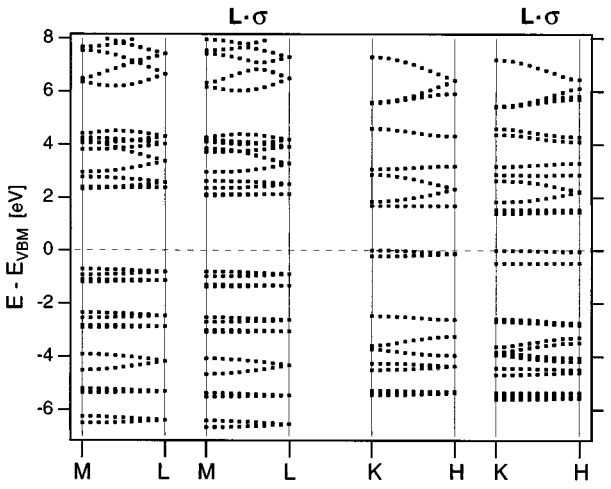

FIG. 3. Effect of spin-orbit ($\mathbf{L}\cdot\sigma$) interaction along the ML and KH lines of the Brillouin zone.

count for polarization effects, which could not be treated self-consistently in their ASW calculation. As a result they obtained the states at K even $\approx$500 meV below those at Γ. Very recently, another band calculation[9] using the relativistic linear muffin-tin orbital method assumed $z=0.125$ and obtained within numerical accuracy a degeneracy between Γ and K (18 meV difference). Like Ref. 7, that work used the atomic sphere approximation.

Restricting ourselves to the measured structure parameters ($z=0.129$) results in the valence-band maximum being located at the edge of the Brillouin zone (K) rather than at its center (Γ), with the rest of the band structure being hardly affected at all. The VBM is now found as much as 170 meV higher in energy than the topmost state at Γ. We should note here that this finding is independent of the inclusion of spin-orbit coupling. This result has important implications for the orbital character of the electronic wave functions at the VBM. Whereas the highest occupied valence band state at Γ consists of hybridized Se $4p_z$ and W $5d_{z^2}$ out-of-plane orbitals [hence its pronounced dispersion along the ΓA (Δ) direction], we find almost exclusively W $5d_{xy,x^2-y^2}$ character[34] for the two topmost bands at K, leading to a very weak dispersion perpendicular to the WSe_2 sheets ($\approx$40 meV). As a consequence, the valence-band edge now appears to be of much more two-dimensional nature than previously suggested, with obvious implications for the conductivity anisotropy of p-doped material.

The detailed behavior of the states at the VBM is strongly affected by spin-orbit interaction. In the absence of relativistic effects it is an important symmetry property of the D_{6h}^4 space group[35] that *all* bands in the AHL plane of the BZ (i.e., $k_\perp = \pm\pi/c$) are twofold (threefold for some bands) degenerate, whereas away from that plane they are generally split due to the interlayer interaction within the 2H unit cell. However, as we will show in Sec. V, experimentally we find this degeneracy to be lifted, particularly near the VBM. Figure 3 contains a comparison of bands along the ML and KH symmetry lines calculated without and with the inclusion of spin-orbit coupling. The effect of the relativistic interaction is most evident along KH. Not only is the degeneracy of the two topmost bands at the H-point lifted, but they also display an almost constant energy separation ($\approx$360 meV) along the entire KH line. In other parts of the BZ, the effect of the spin-orbit interaction is much less important, and along the ML direction the bands seem hardly affected at all (cf. Fig. 3). This result demonstrates again that the band behavior near the $K(H)$ point is most sensitive to a correct theoretical treatment.

The description of the rest of the band structure is straightforward. In the Δ (i.e., ΓA) direction pairs of dispersive bands are observed (cf. Fig. 2), which are derived mainly from out-of-plane orbitals (mostly W $5d_{z^2}$ for the topmost pair and Se $4p_z$ for the other two). In the D_{6h}^4 space group they split up into subbands of Δ_1 and Δ_2 symmetry. The other bands, both occupied and unoccupied, are formed predominantly out of in-plane orbitals and thus display only little dispersion perpendicular to the layers. Away from the Δ line these bands are of strongly hybridized nature. Note, however, that, despite these assignments of the bands to atomic orbitals, a considerable fraction of the weight of the corresponding wave functions is located at interstitial sites, i.e., outside the atomic spheres.

The conduction-band minimum, which is obtained about halfway between Γ and K, consistent with previous calculations and our experimental findings (cf. Sec. V), also shows a pronounced in-layer character like the VBM, so that both are found to be of two-dimensional nature. Se $4p$ states contribute to the unoccupied bands mostly close to the Δ line, whereas the lower-lying unoccupied bands generally have more W $5d$ character. Like for the occupied bands, an important amount of interstitial (strongly delocalized) contribution is found for merely all empty states. Resulting from the use of full potentials and a much better basis set, our calculation yields, compared to previous work,[7] an increased number of conduction bands within the first 5–6 eV above the CBM.

Our calculation thus confirms the indirect character of the fundamental band gap. However, transitions across the gap have to occur between the *K point* and the CBM at $\approx$ 0.5 ΓK and not between Γ and the CBM as suggested previously. The gap size obtained in our calculation is 0.8 eV, considerably smaller than the 1.2 eV obtained from optical absorption.[23] This reflects the usual problem of LDA calculations to describe excitation energies accurately and signals the importance of electron-electron correlation. The smallest direct gap is obtained at the K point and the spin-orbit split bands in its vicinity appear to be good candidates for the formation of the optical A and B excitons.

Partial densities of states (DOS) obtained in our calculation show that both Se $4p$ and W $5d$ states contribute to the entire occupied bandwidth (see Fig. 4), consistent with the above discussion. This yields a much more covalent picture of WSe_2 than originally suggested for the TMDC's by Wilson and Yoffe.[1]

V. SPECTROSCOPIC RESULTS

A. Density of states

The occupied part of the DOS was measured both by x-ray excited photoemission spectroscopy (XPS) on single

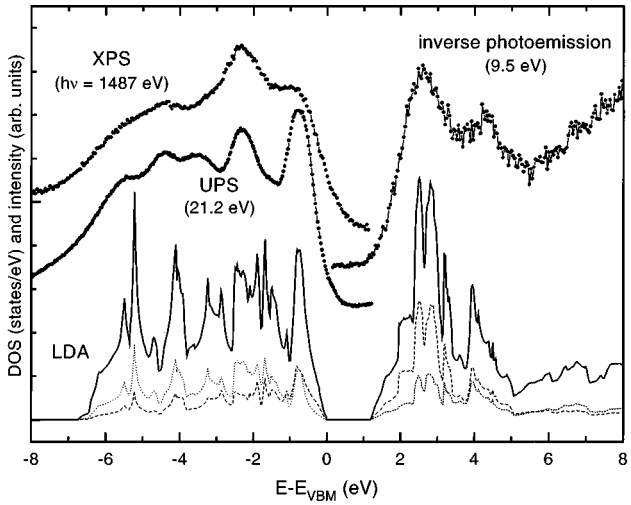

FIG. 4. Densities of states (solid curve, DOS; dashed and dotted curves, partial W and Se DOS, respectively) obtained from the LDA calculation in comparison to **k**-space averaging photoemission (UPS and XPS) and inverse photoemission spectra.

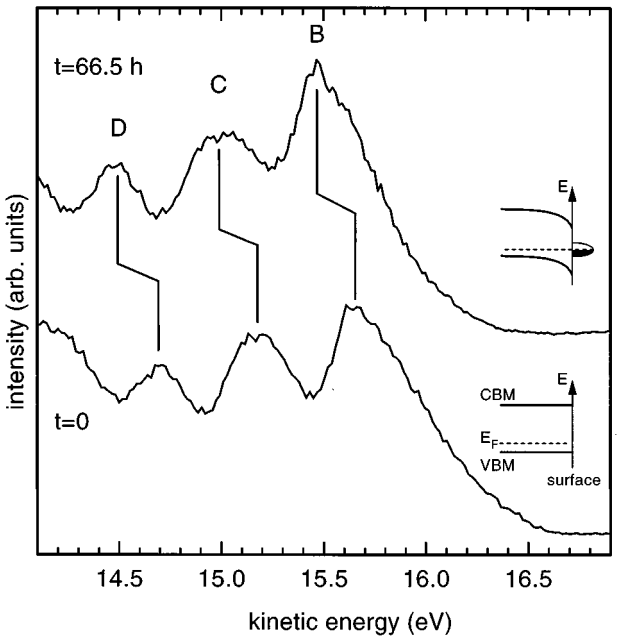

FIG. 5. He I spectrum measured in normal emission as a function of time after cleavage of the crystal. Note the rigid shift to lower energy, caused by defect state-induced band bending in the near-surface region, as shown schematically.

crystals as well as by photoemission using He I radiation [ultraviolet photoemission spectroscopy (UPS)] on polycrystalline samples. The latter were also used for the determination of the empty part of the DOS by inverse photoemission. Figure 4 compares these data to the calculated total DOS and the partial W and Se densities of states per atom. The band gap in the theoretical DOS has been adjusted to the optically measured one.

As can be readily seen from Fig. 4, theoretical and experimental intensities agree rather well, yielding a first confirmation of the quality of the calculated band structure. Also, the structures in the XPS spectrum of a single crystal match nicely those in the UPS data on polycrystalline material. As far as relative intensities are concerned, we note that the structure closest to the Fermi level is more pronounced in the UPS spectrum, indicating an enhanced W 5*d* related weight in this particular energy region.[36] This is indeed expected from our LDA calculations. The otherwise fairly photon energy-independent shape of the Brillouin zone-integrated photoemission spectra confirms the strongly covalent character of the chemical bonding in WSe_2.

B. Time-dependent band bending

Though the surface of WSe_2 is usually viewed as chemically inert,[2] we have observed a pronounced time-dependent energy shift of our photoemission spectra. This is illustrated in Fig. 5, which shows two normal emission spectra of the same sample, one measured immediately after cleavage and the other after almost 3 days of ARPES. Clearly, a rigid shift to lower energies by $\approx$200 meV has occurred. It has previously been demonstrated that immediately after cleavage the WSe_2 surface displays flat-band behavior,[37] because no intrinsic surface states exist on this van der Waals bonded system. However, over the time scale of our measurements (up to several days on the same surface) photon- or adsorbate-induced defect states are apparently created in the band gap, whose density is far below our detection limit but sufficient to cause a band bending at the surface, which serves to compensate for the additional surface charge and satisfy charge neutrality.[38] In fact, it is actually the absence of intrinsic surface states that makes the WSe_2 surface so sensitive to the effect of defect states.

Energy shifts were also observed in our synchrotron radiation experiments. Here the photon energy was varied in order to determine the dispersion perpendicular to the layers (see Sec. V C). Figure 6(a) shows the binding energy (actually the kinetic energy minus the photon energy) of peak *D* (cf. Fig. 5) as function of photon energy. The resulting plot indicates a rather irregular behavior, which cannot be attributed to energy dispersion. We note that the photon energy was not increased in chronological order and indeed the puzzle can be resolved when the energy of *D* is plotted versus time [Fig. 6(b)]. Now a continuous shift to higher binding energy by as much as 250 meV can be identified. Within the first 10 h after crystal cleavage the surface was not exposed to vacuum ultraviolet (vuv) photons except for two quick spectra after about 5 h. During that period the binding energy appears rather stable. However, after that the surface was constantly illuminated with vuv radiation, causing an increasing and eventually saturating energy shift within the next 3–5 h. From this behavior we conclude that the extrinsic surface states responsible for the observed band bending are due to photon-induced defects rather than to surface contamination. This finding is further confirmed by the observation that focusing the photon beam onto a previously unexposed part of the surface immediately restores flat-band behavior.

For a correct interpretation of the spectroscopic results it is important to eliminate these time-dependent energy shifts from the raw data. In the measurements with the He discharge lamp this was achieved by repeatedly measuring normal emission spectra such as in Fig. 5, thus carefully moni-

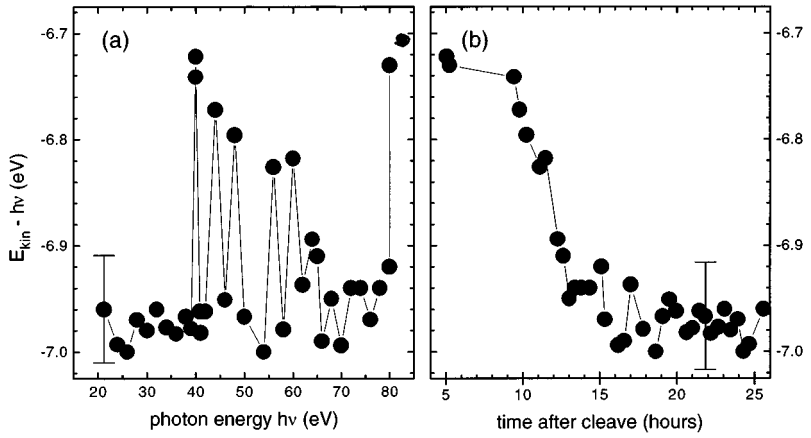

FIG. 6. (a) Energy (E_{kin} - $h\nu$) position of peak D (cf. Fig. 5) in normal emission spectra as a function of photon energy. The error bar indicates the experimental energy resolution. (b) Same as (a), but now plotted versus time after surface preparation.

toring the band bending. In the synchrotron radiation experiments a frequent change of photon energy as required for calibration spectra was undesirable. Instead, we utilized the fact that the energy of peak D in Fig. 6(b) saturates at a fixed value irrespective of the used photon energy. Therefore, its measured binding energy has been used for keeping track of the band bending.

Finally, we note that after even a short exposure of the surface to low-energy electrons (as in ARIPES or LEED) the observed energy shifts were similar to those obtained after a long period of vuv irradiation and showed no or only little further time dependence. This indicates that electron bombardment creates surface defects at a considerably higher rate than the photons, resulting in an almost immediate saturation of the band bending.

C. ARPES in normal emission

Figure 7 displays ARPES spectra measured in normal emission and with synchrotron radiation ranging from 24 to 80 eV. Since the excitation probabilities of the valence electrons vary strongly with photon energy, the spectra have been arbitrarily scaled to about the same maximum height. The photon energy independence of peak D was not only used to compensate the measured energies for band bending, but served also to calibrate the synchrotron data relative to the spectra measured with He I radiation (the corresponding normal emission spectrum is also included in Fig. 7). Apart from relative intensity variations we observe both dispersive (particularly between 0 and -1 eV) and nondispersive features in the spectra. Between $h\nu = 48$ and 54 eV a doublet is seen to move through the valence band, which is due to the excitation of Se $3p$ core electrons by second-order light. At the upper end of the covered photon energy range the spectra seem to become rather independent of the excitation energy.

In order to extract band-structure information from the ARPES data we utilize the fact that in the photoemission process the wave-vector component parallel to the surface is conserved and given by

$$k_{\parallel}(\text{Å}^{-1}) = 0.512\sqrt{E_{\mathrm{kin}}(\text{eV})}\sin\vartheta, \tag{1}$$

where E_{kin} is the kinetic energy of the photoelectron and ϑ its emission angle relative to the surface normal.[39] The component perpendicular to the surface, however, will change when the photoelectron passes through the bulk-vacuum interface. Determining its value inside the crystal requires the knowledge of the final states, which usually can be approximated fairly well by a parabolic energy dispersion, characterized by an inner potential V_0 (measured relative to the vacuum level) and an effective mass m^* (in units of the free-electron mass). This yields

$$k_{\perp} = 0.512\sqrt{m^*(E_{\mathrm{kin}} + V_0) - E_{\mathrm{kin}}\sin^2\vartheta}. \tag{2}$$

Clearly, in normal emission $\vartheta = 0°$ and hence $k_{\parallel} = 0$, and only Eq. (2) applies. By varying the photon energy different kinetic-energy ranges are measured, thus scanning $k_{\perp}$ along the ΓA line of the BZ. V_0 and m^* are determined in such a way as to obtain symmetric energy dispersion about critical points in **k** space. In the literature, values for m^* close to

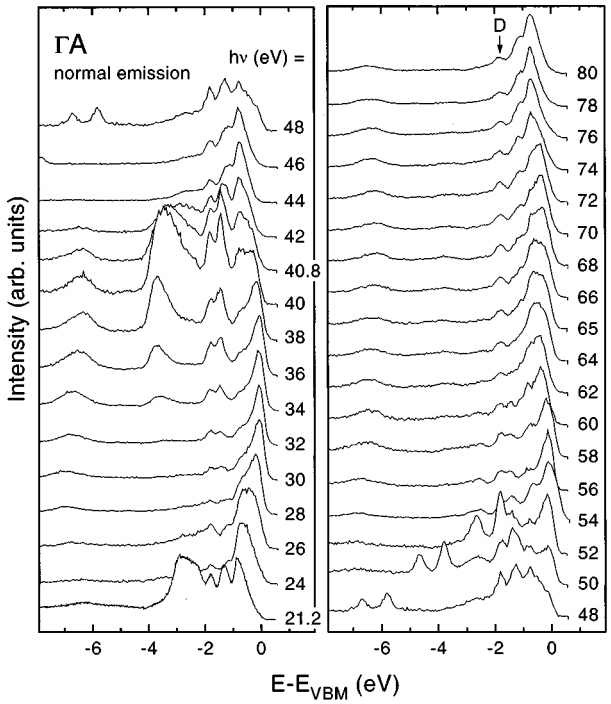

FIG. 7. Normal emission spectra excited with synchrotron radiation of varying photon energy. The data are corrected for band bending by aligning to the nondispersive peak D (see the text for details).

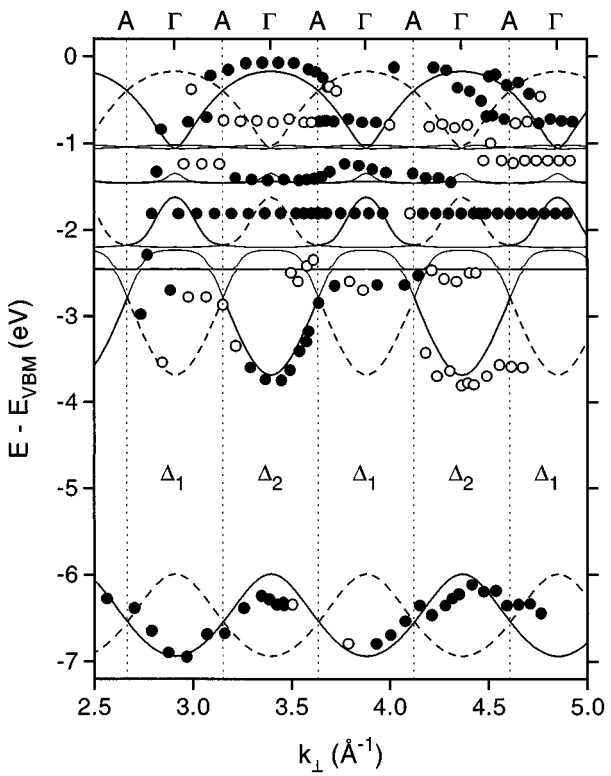

FIG. 8. Comparison of experimental and theoretical band dispersions along ΓA, displayed in the extended zone scheme. Solid and open circles represent strong and weak experimental structures. Theoretical bands, from which photoexcitation into the vacuum is symmetry allowed (forbidden), are indicated by solid (dashed) curves. The allowed symmetries ($\Delta_{1,2}$) are also shown.

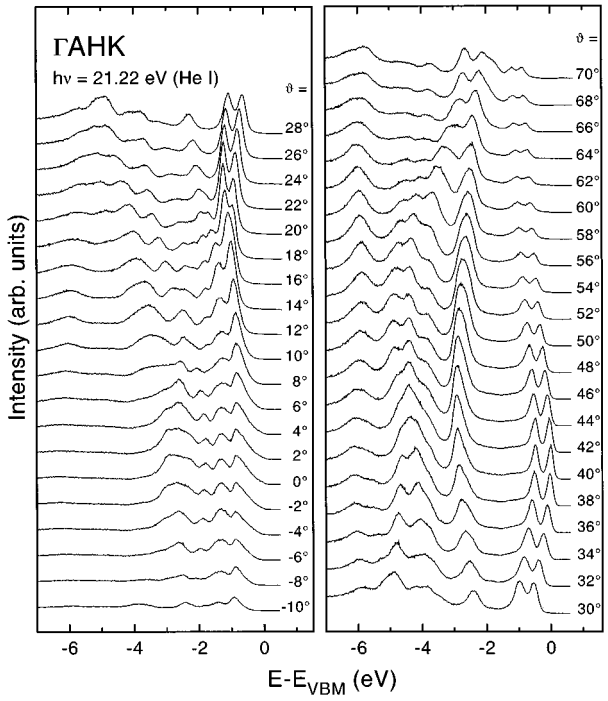

FIG. 9. He I ARPES spectra measured for emission angles ϑ in the ΓAHK plane.

unity and for V_0 of 12 and 14.5 eV have been found for the related compounds $MoSe_2$ and $TiTe_2$, respectively.[7,40] Optimum values for WSe_2 are obtained in the same range, with $m^* = 1.05 \pm 0.05$ and $V_0 = 14.5 \pm 0.5$ eV. These parameters have been confirmed independently by target current spectroscopy.[41]

The resulting experimental band structure is plotted in Fig. 8 together with the theoretical bands, with both measured and calculated energies referred to that of the VBM. From this comparison we obtain good qualitative agreement, particularly for those bands that display a pronounced $k_\perp$ dispersion due to their three-dimensional character. In contrast, the calculated energies of the essentially $k_\perp$-independent bands within the first 2.5 eV of the VBM seem to be off from the measured ones by several 100 meV. Notably, the nondispersive peak at -1.8 eV, which we have used for energy calibration, falls into an energy range where the theory predicts a 0.5-eV-wide band. As mentioned above, the spectra measured at high photon energies display only little energy dispersion. We attribute this to the fact that at these energies the photoelectrons have only a very short mean free path of the order of (or even smaller than) the unit cell extension perpendicular to the surface ($c = 12.96$ Å). In this case the information on $k_\perp$ almost completely smears out, so that the spectra rather reflect a one-dimensional density of states.

While the dispersive valence-band features observed in the low-photon-energy range follow the calculated bands nicely, their periodicity in **k** space seems twice as large as that of the underlying zone scheme. In other words, only every second calculated band is seen in the experiment. This phenomenon is a consequence of a selection rule that is directly related to the existence of a screw axis in the structure of 2H-WSe_2. It was first observed in ARPES on graphite,[12] which has the identical nonsymmorphic space group. As already stated in Sec. IV, in this structure all Bloch states on the ΓA line are of either Δ_1 or Δ_2 symmetry. Group-theoretical considerations show that optical transitions from initial to final states within the crystal are only allowed within the Δ_1 and Δ_2 subgroups, respectively. On the other hand, the even symmetry required for a coupling to a free-electron plane wave at the surface is for a photoelectron state of Δ_1 (Δ_2) only assumed in odd (even) numbered Brillouin zones in the periodic zone scheme.[12] As a result, photoemission from a given valence band can be observed in only every other BZ. In Fig. 8 we have indicated the observable (''forbidden'') theoretical bands by solid (dashed) curves, and it is apparent that the experiment indeed reproduces the expected behavior. We note in passing that due to this effect the first intense peak seen in the He I normal emission spectrum is actually due to the second highest occupied state (Δ_1), with the topmost state (Δ_2) being symmetry forbidden.

D. Off-normal ARPES

Figures 9 and 10 show the angle-resolved He I photoemission data measured in the ΓAHK and ΓALM planes, respectively. No background correction has been applied to the spectra; band-bending effects were corrected as described above. Both sets of spectra are richly modulated and show a pronounced angle dependence, particularly in the ΓAHK

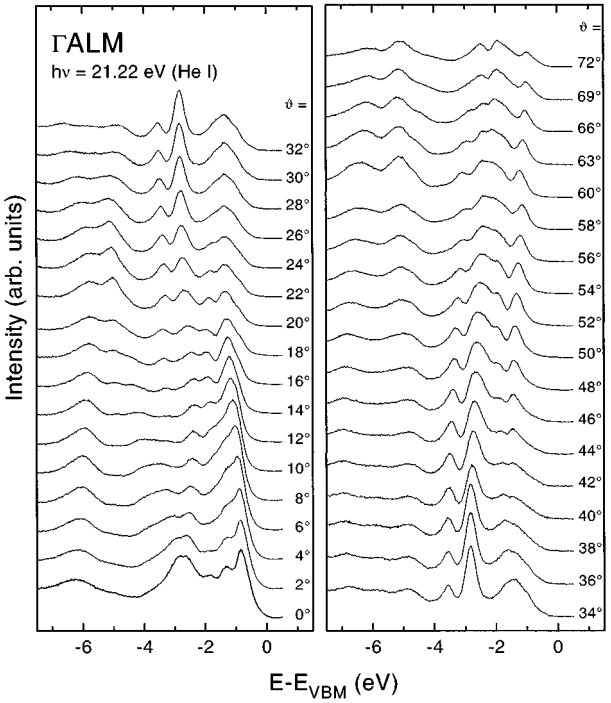

FIG. 10. Same as Fig. 9, but measured in the ΓALM plane.

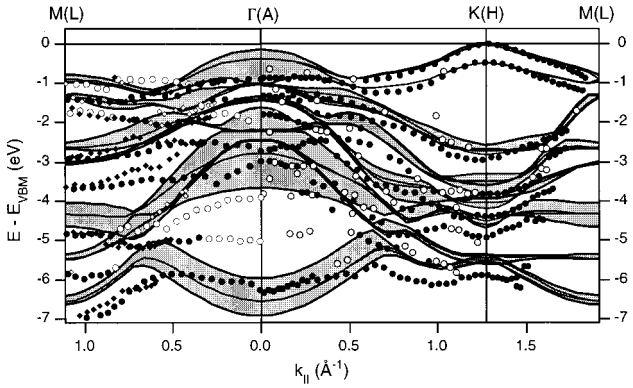

FIG. 11. Experimental energy dispersions measured in the ΓAHK and ΓALM planes compared to the projected LDA volume band structure. Solid (open) symbols denote strong (weak) photoemission features. Circles refer to peaks observed in the first BZ, whereas the position of the diamonds in the ΓALM plane are obtained from folding back from the second BZ. Thick and thin curves represent the calculated band dispersions in the $k_\perp = 0$ and $k_\perp = \pi/c$ planes, respectively.

data. The most prominent spectral feature is the double structure at the top of the valence band in the ΓAHK series, which develops out of a single peak at $\vartheta = 18°$. Towards larger emission angles it disperses by 800–900 meV upward in energy and reaches its maximum at 40°, corresponding to the BZ boundary [$K(H)$ point]. In fact, at this position the upper peak of the doublet is the highest-energy (i.e., lowest-binding-energy) structure in all our ARPES data and we therefore identify its energy with the valence-band maximum. This point will be discussed in more detail in Sec. VI. Here we only note that we have chosen its position as energy zero for all experimental data.

A detailed comparison of the measured and calculated electronic structure can be obtained by plotting the ARPES structures as a function of $k_\parallel$, obtained from Eq. (1), together with the calculated bands (Fig. 11). Since at this level $k_\perp$ is not yet determined, we have included into the plots the theoretical bands of both, the $\Gamma K(\Gamma M)$ and $AH(AL)$ directions, respectively, with the area between corresponding bands being shaded and thus representing a projection of the calculated band structure projected onto the $k_\perp = 0$ plane.

Starting with the ΓALM results we find good qualitative agreement between experimental and theoretical band structures, in the sense that every measured band finds its counterpart in the calculation. The highest observable band displays a slight downward dispersion with increasing $k_\parallel$, as expected from the calculation. As soon as this peak starts to disperse, a shoulder on its low-binding-energy side becomes visible (cf. Fig. 10), which stays at almost constant energy (topmost open symbols in Fig. 11) and is ascribed to indirect transitions out of the high local DOS region around ΓA. At about 3 eV binding energy we observe an experimental peak that seems to remain rather dispersionless in the first BZ (solid circles), but follows the calculated dispersion (though about 0.5 eV too low) in the second BZ (solid diamonds). The origin of this behavior remains unclear. At higher binding energy (≈ 5 eV) a weak structure appears at low emission angles, where a band gap is predicted by the calculation, and merges into a clearly distinguishable feature in correspondence to the calculated bands at larger values of $k_\parallel$. Again, a density-of-states effect could be responsible for this behavior.

In the ΓAHK plane the most striking features are the spin-orbit split W $5d_{xy}$ bands at the top of the valence band and the formation of a large band ''gap'' between them and the lower-lying occupied states at the BZ boundary, i.e., at $K(H)$. With respect to the spin-orbit splitting of the d bands, we obtain almost perfect agreement between theory and experiment. Using V_0 and m^* as obtained from the normal emission data, we can monitor the variation of $k_\perp$ throughout the ΓAHK series and find that, in fact, the AH line is crossed twice in the extended zone scheme (at 24° and 60°, approximately). Our spectra therefore clearly prove the lifting of the degeneracy in the AHL plane by the spin-orbit interaction and confirm the predicted two-dimensional behavior of the W $5d$ bands away from the BZ center. The dispersive behavior of the other valence bands is also in all details well accounted for by the LDA result, except that the calculation seems to underestimate the separation between the W $5d_{xy}$ bands and the following (strongly hybridized) ones by about 0.5 eV. Apart from this deviation we thus find the LDA calculation in excellent accord with our ARPES results.

E. ARIPES

We finally present the 9.5-eV isochromat ARIPES results on the unoccupied bands in WSe_2. Spectra were again measured in the ΓAHK and ΓALM planes and are displayed in Fig. 12. As explained in Sec. II, the energy calibration relative to the VBM was achieved by measuring photoemission spectra on the same surface in the same experimental setting. At normal incidence the inverse photoemission spectrum displays a single peak at about 3.2 eV above the VBM, whose

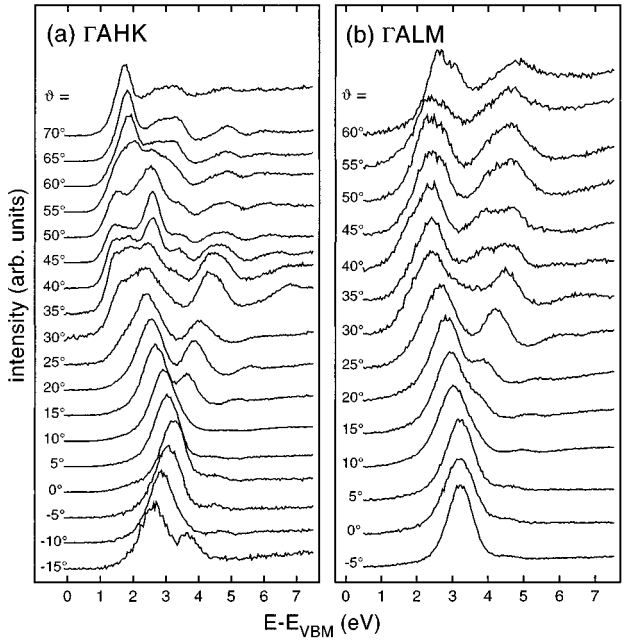

FIG. 12. Angle-resolved inverse photoemission spectra measured in (a) the Γ*AHK* plane and (b) the Γ*ALM* plane. The spectra are normalized to the sample current.

intensity is exceptionally high for this type of experiment, especially relative to the very low ''inelastic'' background. A more careful inspection of the 0° spectrum yields a second, very weak structure at ≈4.6 eV. In the Γ*AHK* series the intense peak splits into two features at 15°, moving up and down in energy, respectively. At even higher incidence angles several distinct peaks develop out of the lower-lying part of the conduction-band emission. The lowest unoccupied state is observed around 40° at ≈1.3 eV relative to the VBM. The spectra measured in the Γ*ALM* plane display a very similar qualitative pattern as a function of electron incidence angle. However, the width of the low-energy band

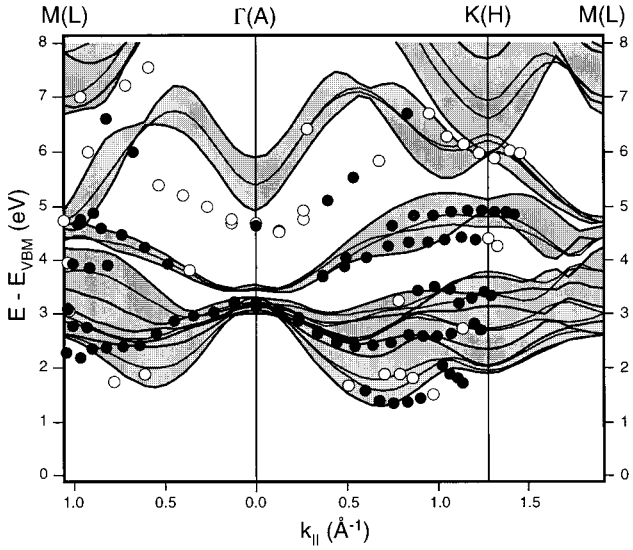

FIG. 13. Comparison of measured and calculated unoccupied bands.

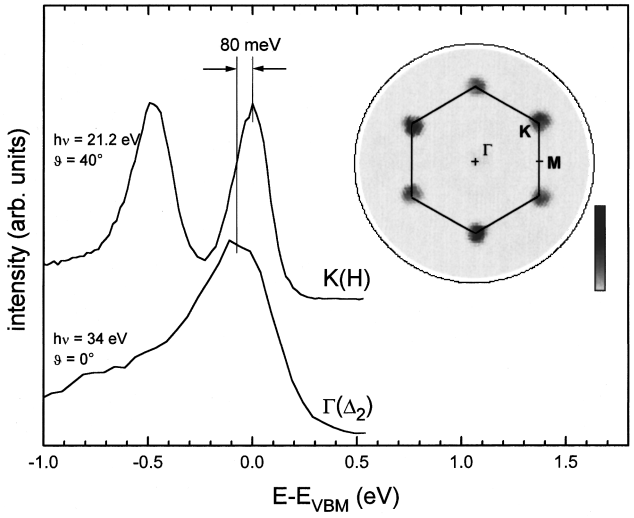

FIG. 14. ARPES spectra measured at $K(H)$ and at the Γ point, demonstrating that the highest occupied state is located at K. Inset: constant energy contours measured at E_{VBM}, visualizing the VBM position in **k** space (see the text for details).

complex is visibly smaller than in the Γ*AHK* series, with the lowest measured energy still by about 0.2–0.3 eV higher than in that plane.

In Fig. 13 we compare the measured conduction-band dispersion to the corresponding LDA bands. Because LDA theory notoriously underestimates the band gap between filled and empty bands we have aligned the theoretical band structure such that it reproduces the experimentally determined gap. With this procedure we obtain good overall agreement also for the unoccupied bands, except for the very weak structure mentioned above, which the theory places 0.5–1.0 eV higher in energy. Looking at the orbital character of the unoccupied bands (cf. Fig. 4), this leads to the same finding as obtained from the ARPES data, namely, that the theory places the hybridized bands somewhat higher in energy relative to the W 5*d* derived states than the experiment. The most important result concerns the **k**-space location of the CBM, which both experiment and theory consistently find at a position halfway between Γ and K.

VI. DISCUSSION

From the above comparison of experimental and theoretical band structures we obtain very good agreement, particularly with respect to the energy-versus-momentum dependence of the valence and conduction bands. Apart from the usual band-gap problem of LDA calculations, the only essential disagreement concerns the relative energies of both occupied and unoccupied W 5*d* derived bands relative to the Se 5*p*/W 5*d* hybrid bands, with the theory placing the latter by about 0.5 eV higher than the measurement. One may speculate whether this deviation is related to the general difficulty of LDA theory to correctly reproduce spectroscopic excitation energies of *d* states,[42] though the effect would be expected to be less pronounced for the relatively delocalized W 5*d* orbitals than, e.g., for open 3*d* shells.

For the determination of the location of the VBM in re-

ciprocal space we compare in Fig. 14 spectra measured at the two critical points Γ and K. They correspond to the local energy maxima of the topmost band measured along the $\Gamma A(\Delta)$ direction and in the ΓAHK plane, respectively. Clearly the highest occupied state is observed at the K point, lying 80 ± 50 meV higher than at Γ, compared to a calculated separation of 170 meV. Strictly speaking, we can only conclude that the VBM is located somewhere on the KH line because the He I, $\vartheta=40°$ spectrum of Fig. 14 does not correspond exactly to the K point [from Eq. (2)]. However, from the theoretical band structure we know that the dispersion of the highest valence band along KH is almost negligible (40 meV) with its energy maximum at K (Fig. 3). Therefore, we can take the measured energy difference between Γ and K as a lower limit. As for the Γ-point spectrum the choice of the photon energy is crucial because the topmost state has Δ_2 symmetry and transitions from it are allowed for $h\nu=34$ eV but symmetry forbidden at 21.2 eV (which would also correspond to a position close to a Γ point). Thus experiment and theory consistently place the VBM at the sixfold degenerate K point (i.e., at the zone edge) of the BZ.

In a very recent similar photoemission study[9] the VBM has been reported to be observed at Γ, lying by 30 meV higher in energy than the topmost state at $K(H)$, in contradiction to our result. We emphasize again that for a correct interpretation of our data it was crucial to account for the time-dependent energy shifts discussed in Sec. V B. As Ref. 9 does not mention the observation of band bending, which we found to be reproducible on all measured samples and also using different spectrometers, we are led to speculate that this effect has gone unnoticed in that work, causing the seemingly conflicting results. Furthermore, the small energy distance between the highest states at Γ and K obtained in Ref. 9 is at variance with optical measurements,[23] which yield a separation of at least 100 meV, much closer to the 80 meV found in this work.

The location of the VBM can be instructively visualized by mapping out a constant energy contour (CEC) at the energy of the VBM. This is achieved by measuring the photoelectron intensity distribution at a given energy as function of the emission direction over the half space above the sample.[8] Apart from matrix element effects, this corresponds to the measurement of band occupancies at the chosen energy in a two-dimensional **k**-space cut. The inset of Fig. 14 shows a CEC map with the energy fixed at E_{VBM}. The intensity spots centred around the six equivalent $K(H)$ points of the BZ mark the highest occupied states in reciprocal space and thus yield a nice illustration of the VBM location. The clarity of this map is helped by the suppression of emission out of the topmost Δ_2 state at Γ at the used photon energy (He I), whose low-energy tail would otherwise contribute some spectral weight at the center of the BZ.

With the VBM at the K point the behavior of the hole carriers in p-doped WSe_2 is expected to be strongly two dimensional, as the states at $K(H)$ are almost exclusively derived from W $5d_{xy}$ and W $5d_{x^2-y^2}$, i.e., in-plane orbitals. From our LDA calculation we obtain an appreciable band mass anisotropy of $m_\perp/m_\parallel\approx4$, whereas holes at the Γ point behave rather isotropically ($m_\perp/m_\parallel\approx1$) due to the sizable contribution of out-of-plane orbitals. Though this finding already accounts for some fraction of the observed transport anisotropy, the major part, however, must still be attributed to carrier scattering. If the underlying microscopic mechanism only involves (quasi)elastic scattering (by impurities or acoustic phonons), the two-dimensional band dispersion near the VBM actually induces an anisotropy also in the scattering rate, as can be shown by a simple phase-space argument. With the VBM at K and negligible dispersion along KH, thermally excited holes will only exist in a narrow energy ''valley'' centered along this line. From the topological shape of the valley it is obvious that the carriers are much more likely to be scattered along the valley axis than perpendicular to it, due to the **k**-space distribution of available scattering final states. This results in an enhanced dissipation of current along the c axis as compared to in-plane directions, yielding a further contribution to the observed transport anisotropy.

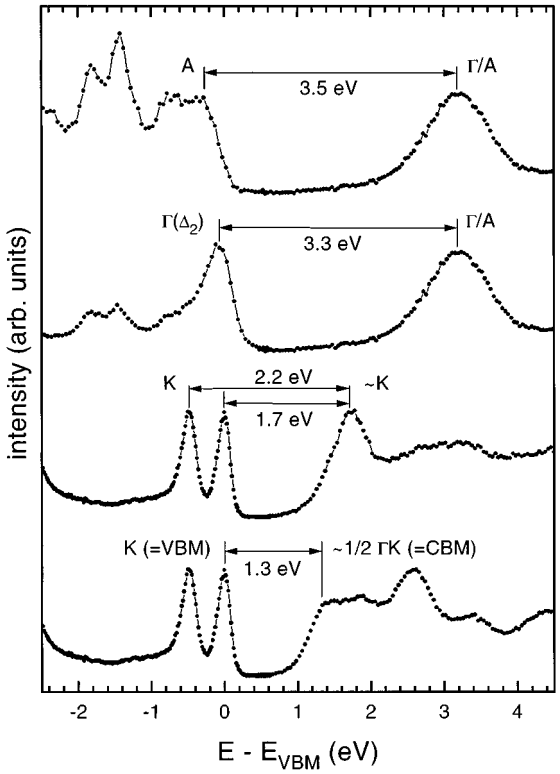

FIG. 15. ARPES and ARIPES spectra measured at selected critical points of the BZ and displayed on a common energy scale, showing the indirect fundamental band gap and the higher-lying direct transitions. The normal incidence ARIPES spectrum is used for both the Γ and the A point, because according to theory the lowest conduction band displays only negligible $k_\perp$ dispersion.

Finally, we can combine the ARPES and ARIPES data on a common energy scale as shown in Fig. 15. We are thus able to measure the band-to-band transition energies at various points in the BZ and to compare these to the optical data. The required energy calibration was already described in Sec. III and results in an overall accuracy of ±0.1 eV for the measured gap energies. As already discussed above, the fundamental band gap involves an indirect transition from the K point to about 1/2 ΓK. From our spectra we determine its size to 1.3 eV, which within our experimental uncertainty agrees well with the 1.2 eV obtained by other groups using

optical spectroscopy[26,23] and combined ARPES/ARIPES.[9] The smallest direct gap is observed at K with a transitionenergy of 1.7 eV, which is in excellent agreement with the energy of the optically measured A exciton (1.71 eV) and therefore confirming the small excitonic binding energy reported previously.[24,25] As the transition from the second-highest state at K occurs at an energy close to that of the optical B exciton (2.2 eV), we find convincing evidence that the A and B excitons are related to direct interband transitions from the spin-orbit split occupied states at K into the lowest empty band. We can thus reconcile the previously reported findings in that we agree with Coehoorn *et al.*[10] on the **k**-space location of the exciton formation and, on the other hand confirm the spin-orbit coupling to be responsible for the measured g-factor dependence.[28] We further note that optical transitions at Γ or A (the same holds for M, etc.) occur at substantially higher energies than at K and agree well with features observed in the optical absorption spectrum.[26]

VII. CONCLUSION

In summary, we have presented an extensive investigation of the occupied and unoccupied electronic structure of the layered semiconductor 2H-WSe_2. We have used ARPES and ARIPES to map out the experimental band structure and obtained very good agreement with our full-potential fully relativistic LDA calculation. The chemical bonding within a WSe_2 trilayer is found to be of strongly covalent nature. The photoemission data display significant band bending upon exposure to the exciting vuv light, presumably caused by photon-induced surface states in the band gap. For a correct interpretation of the spectroscopic energies it is crucial to account for this effect. Most importantly, both experiment and theory place the valence-band maximum at the sixfold degenerate K point of the Brillouin zone, in contrast to previous reports. This results in a strongly two-dimensional character of the VBM and consequently an appreciable band mass anisotropy of the hole carriers in p-doped material. In the calculation the latter effect is strongly enhanced by inclusion of spin-orbit splitting. Combining suitable ARPES and ARIPES spectra, we have determined the band gaps at various locations in **k** space, thus locating the direct and indirect optical absorption thresholds and identifying their origin. The obtained gap energies correlate well with those determined by optical methods. We therefore find that photoemission, optical, and transport properties of 2H-WSe_2 can readily be understood within a single framework.

ACKNOWLEDGMENTS

We wish to thank M. Traving *et al.* for making Ref. 9 available to us prior to publication. This work was supported by the DFG (Sonderforschungsbereich 277 and Grant No. Hu 149/17-1) as well as by the BMBF (Grant No. 13N6602).

*Present address: Institut de Physique, Université de Neuchâtel, CH-2000 Neuchâtel, Switzerland.

†Present address: Institut de Physique Experimentale, EPF Lausanne, CH-1015 Lausanne, Switzerland.

‡Author to whom correspondence should be addressed. Electronic address: claessen@rz.uni-sb.de

§Present address: Hahn-Meitner-Institut, D-14109 Berlin, Germany.

[1] J. A. Wilson and A. D. Yoffe, Adv. Phys. **18**, 193 (1969).

[2] H. Tributsch, Z. Naturforsch. Teil A **32**, 972 (1977).

[3] E. Bucher, M. Lux-Steiner, I. Frankowski, and P. Munz, J. Electrochem. Soc. **85**, 193 (1985).

[4] H. Fuchs and T. Schimmel, Adv. Mater. **3**, 112 (1991).

[5] T. Schimmel, H. Fuchs, S. Akari, and K. Dransfeld, Appl. Phys. Lett. **58**, 1039 (1991).

[6] R. Bromley, R. Murray, and A. Yoffe, J. Phys. C **5**, 759 (1972).

[7] R. Coehoorn *et al.*, Phys. Rev. B **35**, 6195 (1987).

[8] Th. Straub *et al.*, Phys. Rev. B **53**, R16 152 (1996).

[9] M. Traving *et al.*, Phys. Rev. B **55**, 10 392 (1997).

[10] R. Coehoorn, C. Haas, and R. A. de Groot, Phys. Rev. B **35**, 6203 (1987).

[11] W. J. Schutte, J. L. de Boer, and F. Jellinek, J. Solid State Chem. **70**, 207 (1987).

[12] D. Pescia, A. R. Law, M. T. Johnson, and H. P. Hughes, Solid State Commun. **56**, 809 (1985).

[13] L. F. Mattheis, Phys. Rev. **8**, 3719 (1973).

[14] K. K. Kam and B. A. Parkinson, J. Phys. Chem. **86**, 463 (1982).

[15] M. K. Agarwal *et al.*, Cryst. Res. Technol. **19**, 1575 (1984).

[16] M. K. Agarwal, Phys. Status Solidi A **66**, 425 (1981).

[17] W. Kautek, J. Phys. C **30**, L519 (1982).

[18] M. K. Agarwal and P. D. Patel, Phys. Status Solidi A **78**, 103 (1983).

[19] S. Akari *et al.*, J. Microsc. **152**, 521 (1988).

[20] T. Schimmel, H. Fuchs, and M. Lux-Steiner, Phys. Status Solidi A **131**, 47 (1992).

[21] M. Lux-Steiner and T. Schimmel (unpublished).

[22] G. Prasad and O. N. Srivastava, J. Phys. D **21**, 1028 (1988).

[23] K. K. Kam, C.-L. Chang, and D. W. Lynch, J. Phys. C **17**, 4031 (1984).

[24] A. R. Beal and W. Y. Liang, J. Phys. C **9**, 2459 (1976).

[25] A. Anedda, E. Fortin, and F. Raga, Can. J. Phys. **57**, 368 (1979).

[26] A. R. Beal, W. Y. Liang, and H. P. Hughes, J. Phys. C **9**, 2449 (1976).

[27] M. Tanaka, H. Fukutani, and G. Kuwabara, J. Phys. Soc. Jpn. **45**, 1899 (1978).

[28] M. Tanaka, G. Kuwabara, and H. Fukutani, J. Phys. Soc. Jpn. **51**, 3888 (1982).

[29] N. G. Stoffel and P. Johnson, Nucl. Instrum. Methods Phys. Res. Sect. A **234**, 230 (1985).

[30] V. Dose, T. Fauster, and R. Schneider, Appl. Phys. A **40**, 203 (1986).

[31] P. Auer, diploma thesis, Universität des Saarlandes, 1995.

[32] A. Klein *et al.*, Appl. Surf. Sci. **70/71**, 470 (1993).

[33] P. Blaha, K. Schwarz, P. Dufek, and R. Augustyn, computer code WIEN-95, TU Wien 1995 [improved and updated UNIX version of the original copyrighted WIEN code, published by P. Blaha, K. Schwarz, P. Sorantin, and S.B. Trickey, Comput. Commun. **59**, 399 (1990)].

[34] We will, throughout the rest of this paper, refer to this band as the W $5d_{xy}$ band.

[35] C. Herring, Phys. Rev. **52**, 361 (1937).

[36] J. Yeh and I. Lindau, At. Data. Nucl. Data Tables **32**, 1 (1985).
[37] A. Klein *et al.*, Surf. Sci. **321**, 19 (1994).
[38] W. Mönch, *Semiconductor Surfaces and Interfaces* (Springer, Berlin, 1993).
[39] S. Hüfner, *Photoemission Spectroscopy*, edited by M. Cardona, P. Fulde, K. von Klitzing, and H.-J. Queisser, Springer Series in Solid State Sciences Vol. 82 (Springer, Berlin, 1995).
[40] R. Claessen *et al.*, Phys. Rev. B **54**, 2453 (1996).
[41] M. Hengsberger, diploma thesis, Universität des Saarlandes, 1995.
[42] P. Fulde, *Electron Correlations in Molecules and Solids*, edited by M. Cardona, P. Fulde, K. von Klitzing, and H.-J. Queisser, Springer Series in Solid State Sciences Vol. 100 (Springer, Berlin, 1991).